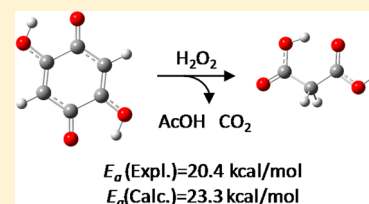# Degradation of 2,5-Dihydroxy-1,4-benzoquinone by Hydrogen Peroxide: A Combined Kinetic and Theoretical Study

Takashi Hosoya and Thomas Rosenau*

Department of Chemistry, University of Natural Resources and Life Sciences, Muthgasse 18, A-1190 Vienna, Austria

Ⓢ *Supporting Information*

ABSTRACT: 2,5-Dihydroxy-1,4-benzoquinone (DHBQ) is one of the key chromophores formed upon aging in cellulosic materials. This study addresses the degradation mechanism of DHBQ by hydrogen peroxide to provide a solid knowledge base for optimization of bleaching sequences aiming at DHBQ removal. Kinetic analysis provided an activation energy (E_a) of 20.4 kcal/mol. Product analyses indicated the product mixture to contain malonic acid, acetic acid, and carbon dioxide. DFT(B3LYP) computation presented a plausible mechanism for the formation of these products from DHBQ. DHBQ forms intermediate **I2k**, having an intramolecular O—O bridge between C-2 and C-5 of the 1,4-cyclohexadione structure. This O—O bond is homolytically cleaved, and the subsequent β-fragmentation of the resulting radical forms ketene and oxaloacetic acid. While ketene yields acetic acid, oxaloacetic acid then gives malonic acid and carbon dioxide through further attack of hydrogen peroxide via an intermediate that is oxidatively decarboxylated. The calculated E_a value (23.3 kcal/mol) in the rate-determining step, i.e., the homolysis of **I2k**, agreed well with the experimental value. There is also a minor pathway in which the spin state changes to triplet during the homolysis of **I2k**; in this way two malonyl radicals are formed that are converted to two molecules of malonic acid.

E_a(Expl.)=20.4 kcal/mol
E_a(Calc.)=23.3 kcal/mol

INTRODUCTION

2,5-Dihydroxy-1,4-benzoquinone (DHBQ) has recently been reported as one of the most important compounds that cause discoloration in cellulosic materials. It is a nearly ubiquitous cellulosic chromophore as it is a prime survivor of bleaching treatments, and it is also found in aged cellulosic matrices as it is regenerated from low-molecular weight breakdown products of cellulose aging.[1] The reason why DHBQ is rather resistant toward bleaching chemicals and "survives" industrial pulp bleaching sequences much longer than other aromatic or quinoid chromophores is its exceptional resonance stabilization. In alkaline media it forms a dianion with highly delocalized double bonds. As most common bleaching agents (ozone, hydrogen peroxide, chlorine dioxide) act primarily by attacking double bonds, this explains the increased resistance of the compound toward oxidative destruction and removal.[1] The chemistry of DHBQ has thus become a point of great interest from several viewpoints: the pulp and paper industries are interested in better, i.e., faster and cheaper, removal of the compound from cellulosic pulps; conservationists working with historic cellulosic matrices are looking for mild and compatible ways for DHBQ destruction; and cellulose scientists search for good methods of DHBQ detection and quantification of its effects on cellulose properties. A better understanding of the reactivity of DHBQ is thus quite important for a general understanding of chemical processes in cellulose aging, bleaching, and general cellulose science. Scheme 1 gives the structure of DHBQ and its resonance-stabilized dianion.

Many previous accounts have addressed the chemistry of DHBQ, which mainly undergoes electrophilic substitution,[2] nucleophilic substitution,[3] and condensation with amines.[4]

Scheme 1. Structures of 2,5-Dihydroxy-1,4-benzoquinone (DHBQ) and Its Resonance-Stabilized Dianion
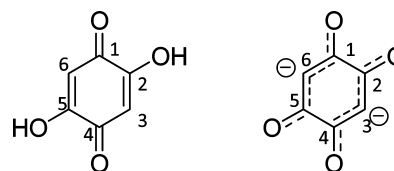
However, these works have employed DHBQ as a starting material in organic synthesis. With the revival of the compound that is connected to its pivotal role in cellulose yellowing, the degradation and "discoloration" of DHBQ became a matter of much interest. It is thus important to investigate the detailed behavior of DHBQ toward bleaching agents and elucidate the compound's degradation mechanisms. In this report, we communicate a clarification of the detailed mechanism of the reaction between DHBQ and hydrogen peroxide as one of the most common bleaching agents, combining experimental investigation with computational studies (DFT calculations).

RESULTS AND DISCUSSION

Kinetic Analysis and Product Characterization. For kinetic studies of the reaction of DHBQ with hydrogen peroxide, a reaction system as simple as possible was chosen, using aqueous, nonbuffered solutions of both reagents. In principle, the reaction follows a second-order rate law. However, if an excess amount of hydrogen peroxide is used

(as under our standard conditions: 257 molar equiv of H_2O_2 relative to DHBQ; see Experimental Details), the rate law assumes a pseudo first order. In this case, the concentration of DHBQ [DHBQ] at reaction time t is presented by the following equation:

$$[DHBQ] = [DHBQ]_0 e^{-kt} \tag{1}$$

where $[DHBQ]_0$ is the initial concentration of DHBQ, and k is the pseudo-first-order rate constant. We can determine k from the slope of the curve that plots $\ln[DHBQ]$ versus t. Figure 1
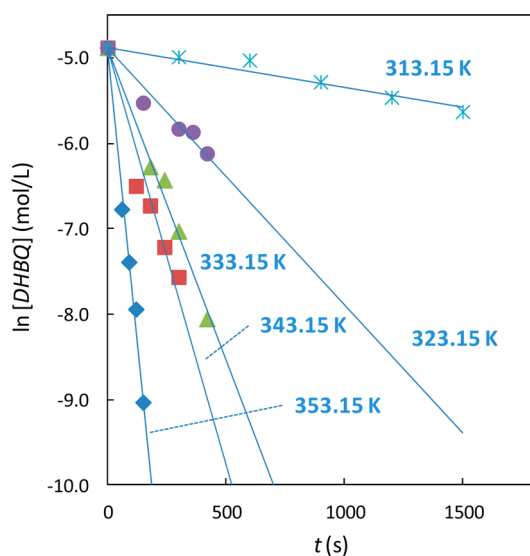

Figure 1. Relationship between $\ln[DHBQ]$ and reaction time t in the temperature range from 313.15 to 353.15 K.

shows such a plot in the range of 313.15−353.15 K. It is evident that there is a linear relationship between $\ln[DHBQ]$ and t, indicating correctness of the pseudo-first-order approximation. The pseudo-first-order rate constant k follows at each temperature from the slope of the lines; the determined k values ranged from 4.66×10^{-4} to 2.74×10^{-2} s^{-1}, as summarized in Table 1.

Table 1. Experimental Pseudo-First-Order Rate Constants (k) and Activation Parameters in the Degradation of DHBQ by H_2O_2 in Non-buffered Aqueous Solution

temp (K)	k (s^{-1})	activation parameter[a]		
		$\Delta^{\ddagger}H°$ (kcal/mol)	$\Delta^{\ddagger}S°$ (cal/mol·K)	$\Delta^{\ddagger}G°$ (kcal/mol)
313.15	4.66×10^{-4}	19.9	−16.3	24.9
323.15	3.01×10^{-3}	19.8	−14.7	24.5
333.15	7.30×10^{-3}	19.8	−14.9	24.8
343.15	9.74×10^{-3}	19.8	−16.2	25.3
353.15	2.74×10^{-2}	19.8	−15.9	25.3

[a]The activation energy (E_a) was determined to be 20.4 kcal/mol.

Figure 2 shows the Arrhenius plot, the logarithm of the pseudo-first-order rate constants k ($\ln k$) versus the reciprocal of the reaction temperature (K), having a linear relationship that allows determination of the various activation factors from this plot. The activation energy (E_a) of the reaction of DHBQ with H_2O_2 was determined to be 20.4 kcal/mol, as presented in Table 1. The activation enthalpies ($\Delta^{\ddagger}H° = 19.8$ to 19.9 kcal/
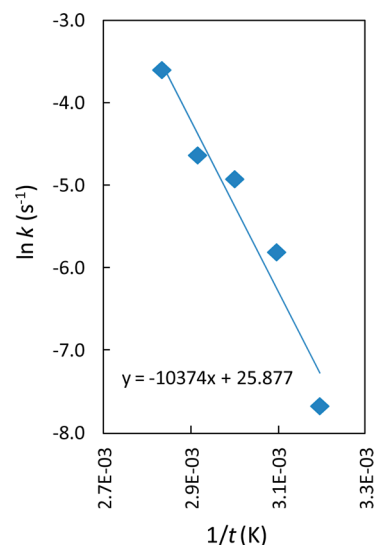

Figure 2. Arrhenius plot of the degradation reaction in the temperature range from 313.15 to 353.15 K.

mol) were very similar to E_a, while the activation Gibbs energies ($\Delta^{\ddagger}G° = 24.9$ to 25.3 kcal/mol) were substantially higher than $\Delta^{\ddagger}H°$ due to negative activation entropies ($\Delta^{\ddagger}S° = -14.7$ to -16.3 cal/(mol·K)). These negative $\Delta^{\ddagger}S°$ values indicate a higher order in the transition state of the rate-determining step.

Through product analysis by ^{1}H NMR after freeze-drying, we found malonic acid to be the major product from DHBQ, as indicated by the singlet at 3.2 ppm, shown in Figure 3A. The presence of malonic acid was also confirmed by GC−MS analysis; see Figure S1 in Supporting Information for the total-ion chromatogram and the mass fragmentation pattern of the trimethylsilyl (TMS) derivative. The carbon-based yield of malonic acid was not quantitative but was almost constant under the employed reaction conditions (44.4−55.1%); see Table S1 in Supporting Information for the yield of malonic acid under each reaction condition. This result indicates that H_2O_2-degradation of DHBQ forms other major products that were undetectable by either ^{1}H NMR or GC−MS after freeze-drying.

To identify those byproducts, *in situ* ^{1}H NMR analysis of the reaction in D_2O was performed. As shown in Figure 3B, a singlet at 1.88 ppm appeared, which did not occur in the ^{1}H NMR spectrum (DMSO-d_6) after freeze-drying (Figure 3A). From its chemical shift, the signal was assigned to acetic acid (confirmed by spiking), which was volatile enough to be evaporated from the product mixture during the freeze-drying process. It was likely that acetic acid was not produced as the decarboxylation product of malonic acid, but directly from DHBQ, since malonic acid was found to be considerably stable under the reaction conditions and formed only rather minor amounts of acetic acid at 313.15 K over a prolonged reaction time (1 day); see Figure 3C. The acetic acid formed was not quantified as we were unable to find a suitable internal standard that additionally was stable enough toward hydrogen peroxide.[5]

Adding the reaction mixture into a saturated aqueous solution of calcium hydroxide resulted in formation of white precipitate; see Figure S2 in the Supporting Information. This indicated the presence of carbon dioxide (carbonate) in the reaction mixture. Since carbon dioxide is also formed from malonic acid (decarboxylation) and acetic acid (minor
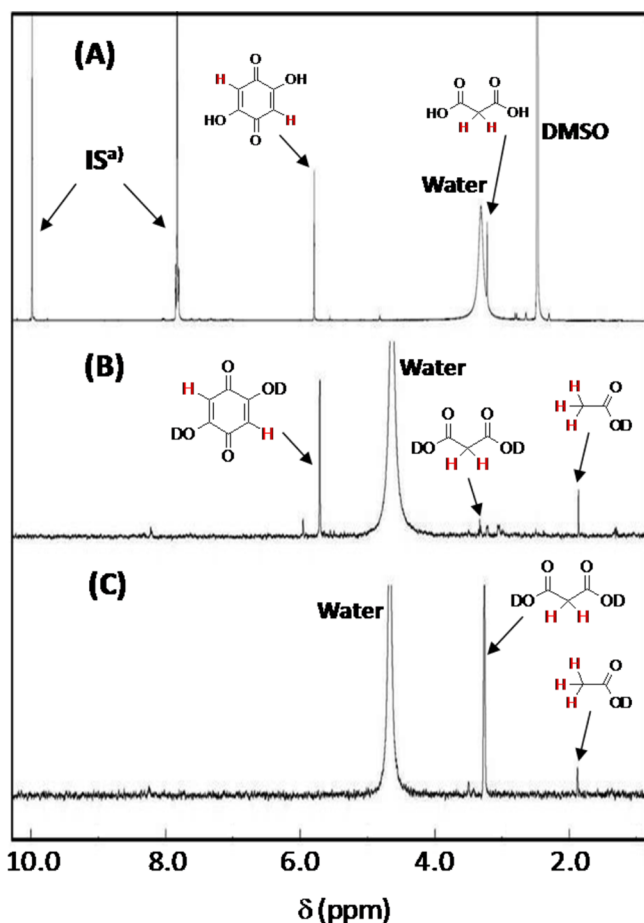
Figure 3. ^{1}H NMR spectrum in DMSO-d_6 of (A) the product mixture after freeze-drying (313.15 K/300 s), (B) the in situ reaction mixture from DHBQ in D$_2$O (313.15 K/300 s), and (C) the reaction mixture in the degradation of malonic acid in D$_2$O (315.15 K/1 day). Note: [a]IS = internal standard (4-bromobenzaldehyde).

oxidation) under the same conditions, it was unclear at this moment whether carbon dioxide was produced directly from DHBQ. However, in the next section, we will clarify this issue, showing that carbon dioxide is already formed in the degradation of DHBQ to malonic acid.

As a summary of the experiments, we found that DHBQ degrades mainly into malonic acid with a carbon yield of ∼50% in the aqueous hydrogen peroxide solution. Acetic acid and carbon dioxide were also detected but were not quantified. The activation parameters from the Arrhenius plot were E_a = 20.4 kcal/mol, $\Delta^{\ddagger}H^{\circ}$ = 19.8 to 19.9 kcal/mol, $\Delta^{\ddagger}S^{\circ}$ = −14.7 to −16.3 cal/mol·K, and $\Delta^{\ddagger}G^{\circ}$ = 24.9 to 25.3 kcal/mol.

Computational Study (DFT). Since the kinetic experiments provided only limited information about the detailed mechanism of the degradation, we carried out quantum chemical computations at the DFT(B3LYP) level of theory to elucidate the sequence of elemental reaction steps. First, a test calculation for hydrogen peroxide was carried out to check the performance of the B3LYP functional for the description of the properties of the O−O bond: the DFT(RB3LYP) method correctly presented the geometry of hydrogen peroxide, and the DFT(UB3LYP) method well described the potential energy curve of the cleavage of the O−O bond. Previous work showed that the B3LYP/6-31+G** level of theory successfully reproduced the varying bond lengths within DBHQ that have

been found in crystal structures.[1e] We concluded that we can employ the DFT(RB3LYP) method for the calculation of the equilibrium structures and the transition state of ionic reactions and the DFT(UB3LYP) method for the calculation of the radicals and the transition state of homolytic processes in the reaction system; see the Supporting Information for a detailed discussion of the accuracy of the DFT(B3LYP) method.

Figure 4 shows the overall reaction pathway derived from the DFT(B3LYP) computations: DHBQ (6 carbon atoms) gives malonic acid (3 carbon atoms), acetic acid (2 carbon atoms), and carbon dioxide (1 carbon atom) as reaction products. In the initial step of this degradation, hydrogen peroxide attacks C-2 of DHBQ in a nucleophilic manner to form intermediate **I1e** via transition state **TS1**. In this nucleophilic attack, a proton relay from hydrogen peroxide to the C-4 carbonyl group occurs via three water molecules,[6] as shown in Scheme 2; see also Figure S5 in Supporting Information for detailed geometry changes. The E_a and the $\Delta^{\ddagger}H^{\circ}$ of this step were calculated to be 14.0 and 11.5 kcal/mol, respectively. The $\Delta^{\ddagger}G^{\circ}$ (28.7 kcal/mol) of this step is much higher than the $\Delta^{\ddagger}H^{\circ}$ due to the decrease in entropy by the bond formation between DHBQ and hydrogen peroxide.

After **I1e** is converted into more stable **I1k**, which has a keto structure,[7] O-7′ of **I1k** nucleophically attacks C-5 to form an intermediate **I2e** with 2,5-dihydoxy-1,4-cyclohexadione structure, which has an intramolecular O−O bridge between C-2 and C-5. This intramolecular substitution involves the formation of an anionic intermediate **IA** via **TS2₁** and the nucleophilic attack of anionic O-7′ of **IA** at C-5 via **TS2₂**, as shown in Scheme 3 and Figure 4; see also Figure S6 in Supporting Information for detailed geometry change. E_a and $\Delta^{\ddagger}H^{\circ}$ of this process, i.e. the values for **TS2₂**, are 12.5 and 9.8 kcal/mol, respectively, while $\Delta^{\ddagger}G^{\circ}$ (26.6 kcal/mol) is once more much higher due to the decreased entropy compared to that of the reactants. **I2e** then gives the more stable **I2k** through keto−enol interconversion.[7] We also found another reaction pathway starting from **I1k**, where initial homolysis of the O−O bond of **I1k** occurs, but the E_a of this pathway is so high (29.6 kcal/mol) that this pathway would in fact be negligible; see Figure S7 for the transition state geometry and its energy.

The following step of the overall degradation includes the homolysis of the O−O bond of **I2k** and the β-fragmentation of the resulting radical to form ketene and oxaloacetic acid (**I3**) via **TS3**, as shown in Figure 4. See also the schematic reaction in Scheme 4, the detailed mechanism of which will be discussed later. Ketene is so reactive that it will be readily attacked by water to give acetic acid, which was also detected in the experimental product analysis; see previous section. The DFT(UB3LYP)-calculated energy of **TS3** (E_a = 23.3 kcal/mol, $\Delta^{\ddagger}H^{\circ}$ = 22.4 kcal/mol, $\Delta^{\ddagger}G^{\circ}$ = 33.4 kcal/mol) is considerably higher than those of **TS1**, **TS2₁**, and **TS2₂**, and this process is extremely exothermic; ΔE = −95.0 kcal/mol, ΔH^0 = −96.0 kcal/mol, ΔG^0 = −91.0 kcal/mol. From these results, we concluded that this process evidently is the rate-determining step in the overall degradation. The calculated E_a (23.3 kcal/mol) and $\Delta^{\ddagger}H^{\circ}$ (22.4 kcal/mol) were in quite satisfying agreement with those obtained from kinetic analysis (see Table 1), indicating the correctness of the computed pathway. Though the calculated $\Delta^{\ddagger}S^{\circ}$ (−36.6 kcal/mol) value is not in quantitative agreement with that of the experiment (−16.3 kcal/mol, see Table 1), the largely negative $\Delta^{\ddagger}S^{\circ}$ was well reproduced by the DFT(B3LYP) computation.[8] Note that geometry optimization of the biradical produced from the O−
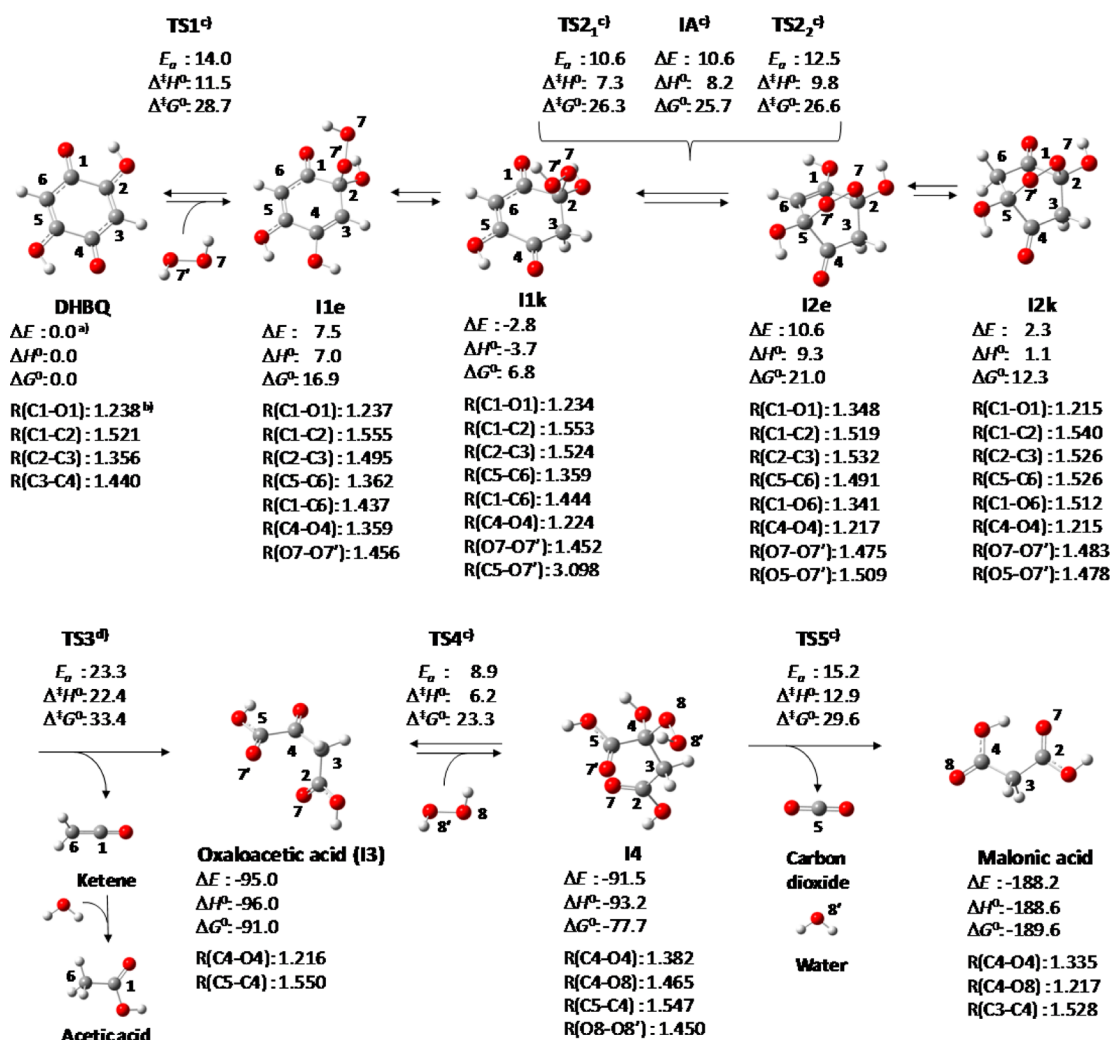
Figure 4. Reaction pathway from DHBQ to malonic acid calculated with DFT(B3LYP) method. Notes: [a] Energies are presented in kcal/mol. [b] Bond lengths are presented in Å. [c] The energies of these transition states and intermediates are calculated relative to the DHBQ-3H$_2$O complex instead of DHBQ; see Figure S4 in Supporting Information for the geometry of the DHBQ-3H$_2$O complex. [d] DFT(UB3LYP) method was employed for the energy evaluation of **TS3**; see also Figure S3 in Supporting Information.

Scheme 2. Nucleophilic Attack of Hydrogen Peroxide to DHBQ
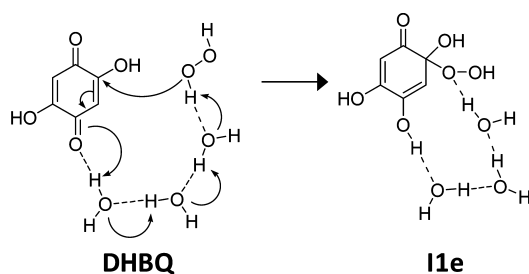
Scheme 3. Intramolecular Nucleophilic Attack in I1k To Form I2e
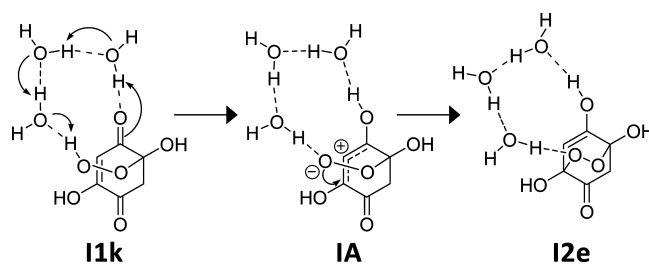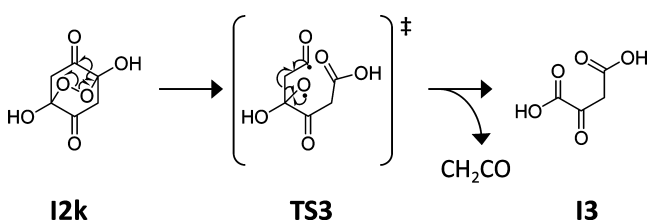

O bond cleavage of **I2k** was not successful, resulting in the reformation of the O−O bond again. This means that the biradical is not a stable species and exists only transitorily in the reaction course from **I2k** to ketene and **I3**.

The next step of the sequence is a further nucleophilic attack of hydrogen peroxide to the carbonyl group of oxaloacetic acid (**I3**) to form intermediate **I4** via **TS4**; see Figure S8 in Supporting Information for detailed geometry changes. The E_a, $\Delta^{\ddagger}H°$, and $\Delta^{\ddagger}G°$ values of this process were 8.9, 6.2, and 23.3

kcal/mol, respectively, relative to oxaloacetic acid (**I3**). **I4** then releases carbon dioxide and water to yield malonic acid with an E_a of 15.2 kcal/mol, $\Delta^{\ddagger}H°$ of 12.9 kcal/mol, and $\Delta^{\ddagger}G°$ of 29.6 kcal/mol via **TS5**; see Figure S9 in Supporting Information for detailed geometry changes. The activation barrier in **TS5** is higher than that in **TS4**. The step from **I4** to malonic acid and carbon dioxide via **TS4** is thus the rate-determining step with regard to the degradation of oxaloacetic acid (**I3**). The activation barrier to **TS5** (E_a = 15.2 kcal/mol, $\Delta^{\ddagger}H°$ = 12.9 kcal/mol, $\Delta^{\ddagger}G°$ = 29.6 kcal/mol) is much lower than that to

Scheme 4. Schematic Description of the Mechanism in the Rate-Determining Step

Figure 6. NBO charge and Mulliken spin density of important atoms of **TS3**, calculated with the DFT(UB3LYP) method. Note: [a] The values in parentheses are the difference in NBO charge relative to **I2K**.

TS3 (E_a = 23.3 kcal/mol, $\Delta^{\ddagger}H^{\circ}$ = 22.4 kcal/mol, $\Delta^{\ddagger}G^{\circ}$ = 33.4 kcal/mol, see Figure 4). Hence, it is reasonable to assume that oxaloacetic acid (**I3**), once formed, is rapidly degraded and was thus not detected in the experiment. It should be also noted that the reaction from oxaloacetic acid (**I3**) to malonic acid is known as a general method for oxidative decarboxylation of an α-keto acid and that a previous experimental study about its degradation mechanism well supports the presented mechanism.[9]

In the overall reaction, homolysis of the O−O bond of **I2k** and the subsequent β-fragmentation of the resulting radical via **TS3** is the most important process, which is also the rate-determining step as discussed above. Therefore, we should like to address the detailed mechanism of this step. Figure 5 shows the geometry changes in the reaction from **I2k** to ketene and oxaloacetic acid (**I3**). From **I2k** to **TS3**, the O-7−O-7′ bond is considerably elongated from 1.483 to 2.091 Å, as is the C-1−C-2 bond from 1.540 to 1.836 Å, while the O-7−C-2 distance is shortened form 1.478 to 1.301 Å. Despite those large geometry changes, the NBO charges of several important atoms are not changed very much, as shown in Figure 6. These results indicate that O-7−O-7′ cleavage is homolytic (radical) rather than heterolytic (ionic). It is noted that the C-1−C-6, C-5−C-6, and C-5−O-7′ bonds are not very different in length between **I2k** and **TS3**. It is thus likely that the reaction from **I2k** to **TS3** is the process where the homolysis of the O−O bond results in the formation of an O-7′-centered radical and an C-1-centered acyl radical, formed through β-fragmentation of the O-7-centered radical, as shown in Scheme 4. This proposal is also supported by high spin densities at O-7, C-1, and O-1 in **TS3**, as shown in Figure 6. From **TS3** to the product complex (ketene and oxaloacetic acid (**I3**)), the C-1−C-6 distance is shortened from 1.513 to 1.312 Å and the C-5−O-7′ distance from 1.384 to 1.211 Å, while the C-5−C-6 distance is elongated from 1.526 to 3.210 Å. These results indicate that the reaction from **TS3** to the product complex involves the β-fragmentation

of the C-1-centered acyl radical to form ketene and oxaloacetic acid (**I3**), as shown in Scheme 4.

According to the mechanism discussed above, the carbon-based yield of malonic acid must be exactly 50%, since one molecule of DHBQ gives one molecule of malonic acid. However, as mentioned in the previous section, the maximum yield of malonic acid was slightly above 50% in some cases; see also Table S1 in Supporting Information. This fact led us to investigate an alternative reaction pathway in which one molecule of DHBQ yielded two molecules of malonic acid. As shown in the potential energy curve for the O-7−O-7′ distance of **I2k** in Figure 7, the potential energy of the singlet state is increased by the elongation of the O-7−O-7′ bond, while that of the triplet state becomes smaller. These singlet and triplet potential energy curves meet around a O-7−O-7′ bond length of 2.0 Å. The spin state of the reactant is thus likely to change from singlet to triplet through a conical intersection when the O-7−O-7′ bond is elongated to around 2.0 Å; see **CI** in Figure 7. When the spin state becomes a triplet, furthermore, the reactant produces two molecules of malonyl radical, as shown in Figure 7, and the malonyl radical would be easily converted into malonic acid, according to the literature.[10] The potential energy of **CI** was calculated to be 25.9 kcal/mol relative to DHBQ, which value is moderately larger than the E_a value (23.3 kcal/mol) of **TS3**. It is therefore likely that this pathway involving the spin state change is one of the minor competitive pathways, occurring as alternative to the one shown in Figure 4. The involvement of this minor path explains
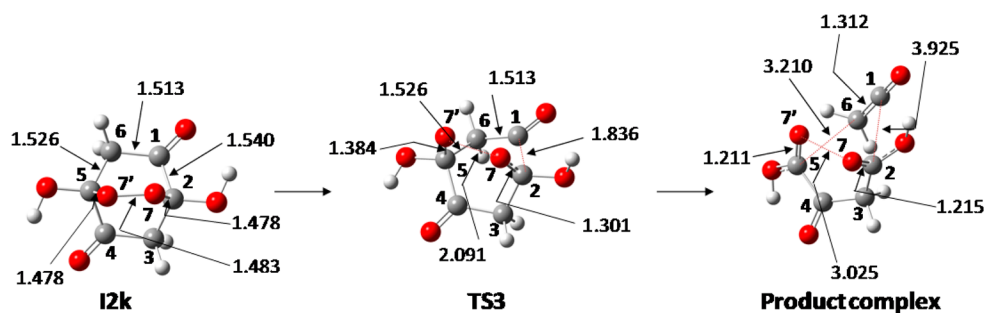

Figure 5. Geometry changes in the rate-determining step calculated with the DFT(B3LYP) method. The bond lengths are presented in Å. The product complex is the IRC product from **TS3**.
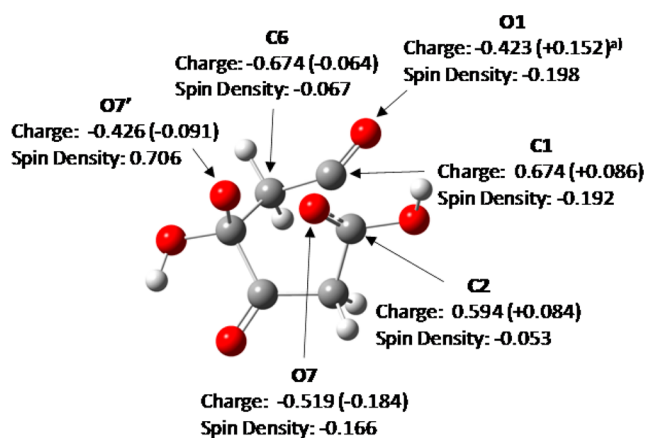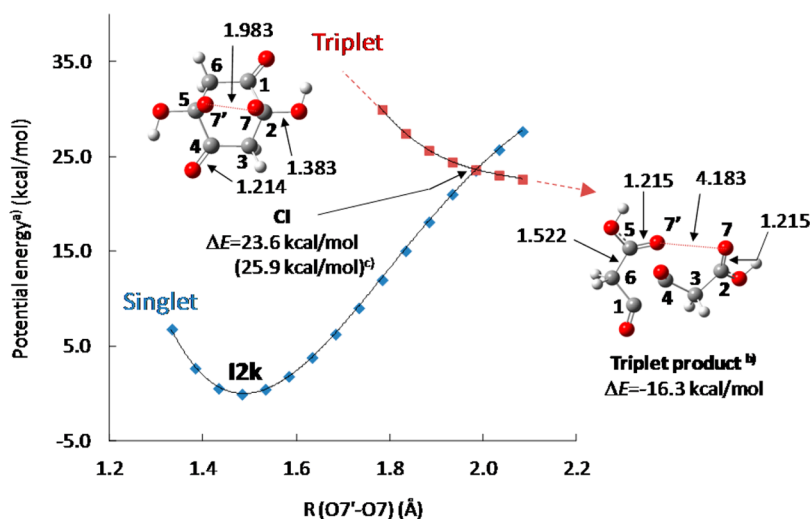
Figure 7. Potential energy curves in singlet and triplet spin states in **12k** in relation to the O-7—O-7′ bond length, calculated with the DFT(UB3LYP) method. The potential energy curves were obtained by free geometry optimizations with the O-7—O-7′ bond fixed at each length. Notes: [a]The potential energy of **I2K** is set to zero here. [b]The triplet product was calculated with the steepest descend optimization starting from **CI** geometry. [c]Potential energy relative to DHBQ is given in parentheses.

the experimental yield of malonic acid ranging slightly above 50%.

CONCLUSIONS

We have investigated the degradation mechanism of DHBQ by hydrogen peroxide in aqueous, nonbuffered medium. Kinetic analysis and product investigation showed DHBQ to afford malonic acid, acetic acid, and carbon dioxide, with an experimental E_a value of 20.4 kcal/mol. DFT(B3LYP) computation indicated that the initial step of this degradation is the formation of intermediate **I2k** with a 2,5-dihydroxy-1,4-cyclohexadione structure having an intramolecular O—O bridge between C-2 and C-5. The O—O bond of **I2k** is then homolytically cleaved, and the resulting radical undergoes β-fragmentation to give ketene and oxaloacetic acid. This process is the rate-determining step in the overall sequence. While ketene is attacked by water to yield acetic acid, oxaloacetic acid suffers rapid oxidative decarboxylation to malonic acid with concomitant release of carbon dioxide and water. The calculated E_a value (23.3 kcal/mol) was in good agreement with the experimental value, indicating the correctness of the computed mechanism. We also found another minor pathway, where the spin state changes from singlet to triplet by the elongation of the O—O bond of **I2k** to give two malonyl radicals, which would be readily converted into malonic acid.

The reaction mechanism allows some direct conclusions as to bleaching sequences in pulp discoloration treatments. By degradation of DHBQ, organic acids are produced that will contribute to a decreased pH value. It is thus recommendable to exert pH control or work in slightly alkaline medium to neutralize the formed acids. Malonic acid is a synthon with high methylene activity and readily undergoes aldol-type condensations. Such reactions might produce potent chromophores (conjugated systems) and thus contribute to unstable brightness in the cellulosic pulps. To avoid this fast brightness reversion, a thorough washing of the pulp to remove all malonic acid is paramount. An ozone bleaching step, which generates high amounts of low-molecular weight carbonyl compounds as potential reaction partners for residual malonic acid, should thus be avoided as last step of the bleaching sequence.

Future studies, to be reported as follow-up of this account, will consider the influence of the reaction pH on the rate and the mechanism of the degradation of DHBQ by H_2O_2.

EXPERIMENTAL AND COMPUTATIONAL DETAILS

Experimental Details. All chemicals were purchased from commercial providers. They were of highest purity available (p.a. grade) and were used without purification. Proton nuclear magnetic resonance (^{1}H NMR) spectra were recorded on at 400.13 MHz proton resonance frequency.

The degradation reaction was started by adding a 30% aqueous solution of hydrogen peroxide (0.22 mL, 1.96 mM hydrogen peroxide) to 2.0 mL of an aqueous solution of DHBQ (1.07 mg, 0.00763 mM) in a 20 mL round-bottom flask. The solution of DHBQ was preheated at temperatures between 313.15 and 353.15 K before addition of the hydrogen peroxide solution. After the reaction mixture was stirred for 60—1800 s, the flask was put into an ice bath to stop the reaction and then was stored at 193.15 K overnight. After freeze-drying of the sample, the residue was analyzed with ^{1}H NMR (DMSO-d_6) and gas chromatography—mass spectrometry (GC—MS, after trimethylsilylation; see below for the procedure). For quantification, 4-bromobenzaldehyde was used as the internal standard. The trimethylsilylation was carried out according to the following protocol: 500 μL of pyridine containing 1.5 mg of N,N-dimethy-4-amino-pyridine was added to the freeze-dried sample, followed by the addition of 500 μL of N,O-bis(trimethylsilyl)trifluoroacetamide containing 10% of trimethylsilyl chloride. The reaction mixture was left at 323.15 K for 2 h to complete the reaction and was then injected directly.

For *in situ* ^{1}H NMR analysis of the reaction mixture, the degradation of DHBQ was performed in D_2O with the same experimental procedure as described above. After the reaction was quenched in the ice bath, the sample was immediately transferred into a NMR tube under further cooling and analyzed by ^{1}H NMR.

For qualitative evaluation of carbon dioxide in the reaction mixture, 20 μL of the reaction mixture was added into a saturated aqueous solution of calcium hydroxide to observe the formation of a white precipitate of $CaCO_3$.

Computational Details. The GAUSSIAN 09 program packages were employed in these calculations.[11] The geometry optimization and energy evaluation was carried out by the DFT method with the B3LYP functional[12] and the PCM method in water. In the geometry optimization, we used the key word "Opt" in GAUSSIAN 09 in case of the calculations of the reactant, products, and intermediates. For the

transition states, we also employed the "Opt" keyword, but additionally set the "Ts", "Noeigentest", and "Calcfc" options; see the manual for GAUSSIAN 09 for the details of these descriptions.[11] The 6-31G(d) basis sets were employed for H, C, and O, where a diffuse function was added to each of O and a p-polarization function was added to H. In all calculations, the solvation energy was evaluated with the PCM method, where the UFF parameters were used to determine the cavity size. It was ascertained that each equilibrium geometry exhibited no imaginary frequency and each transition state exhibited one imaginary frequency. In the case of homolytic cleavage of the covalent O−O bond, the energy was evaluated using the unrestricted-B3LYP (UB3LYP) method instead of the restricted-B3LYP (RB3LYP) one.

Enthalpy, entropy, and Gibbs energy changes were calculated at 293.15 K. Zero-point energy, thermal energy, and entropy change were evaluated with the DFT(B3LYP) method. The translational entropy in water was computationally treated according to the literature.[13] We presented an example of the input file used for the geometry optimization of **TS3** in Supporting Information.

ASSOCIATED CONTENT

Ⓢ Supporting Information

Complete ref 11. Additional experimental details and results. Cartesian coordinates of the optimized geometries. This material is available free of charge via the Internet at http://pubs.acs.org.

AUTHOR INFORMATION

Corresponding Author
*E-mail: thomas.rosenau@boku.ac.at.
Notes
The authors declare no competing financial interest.

ACKNOWLEDGMENTS

REFERENCES

(1) (a) Rosenau, T.; Potthast, A.; Milacher, W.; Hofinger, A.; Kosma, P. *Polymer* **2004**, *45*, 6437. (b) Rosenau, T.; Potthast, A.; Milacher, W.; Adorjan, I.; Hofinger, A.; Kosma, P. *Cellulose* **2005**, *12*, 197. (c) Rosenau, T.; Potthast, A.; Kosma, P.; Suess, H.-U.; Nimmerfroh, N. *Holzforschung* **2007**, *61* (6), 656. (d) Krainz, K.; Potthast, A.; Suess, U.; Dietz, T.; Nimmerfroh, N.; Rosenau, T. *Holzforschung* **2009**, *63* (6), 647−656. (e) Rosenau, T.; Potthast, A.; Krainz, K.; Yoneda, Y.; Dietz, T.; Shields, Z. P. I.; French, A. D. *Cellulose* **2011**, *18* (6), 1623.

(2) (a) Brassard, P.; L'Ecuyer, P. *Can. J. Chem.* **1958**, *36*, 1346. (b) Nicolaides, D. N.; Gautam, D. R.; Litinas, K. E.; Papamehael, T. *J. Chem. Soc., Perkin Trans. 1* **2002**, 1455. (c) Lang, M.; Muhlbauer, A.; Jagers, E.; Steglich, W. *Eur. J. Org. Chem.* **2008**, *20*, 3544. (d) Shaabani, A.; Ghadari, R.; Sarvary, A.; Rezayan, A. H. *J. Org. Chem.* **2009**, *74*, 4372. (e) Shaabani, A.; Ghadari, R.; Ghasemi, S.; Pedarpour, M.; Rezayan, A. H.; Sarvary, A.; Ng, S. W. *J. Comb. Chem.* **2009**, *11*, 956. (f) Misiolek, A. W.; Ichimura, A. S.; Gentner, R. A.; Huang, R. H.; McCaffrey, V. P.; Jackson, J. E. *Inorg. Chem.* **2009**, *48*, 9005. (g) Jimenez-Alonso, S.; Estevez-Braun, A.; Ravelo, A. G.; Zarate, R.; Lopez, M. *Tetrahedron* **2007**, *63*, 3066. (h) Jimenez-Alonso, S.; Perez-Lomas, A. L.; Estevez-Braun, A.; Martinez, F. M.; Orellana, H. C.; Ravelo, A. G.; Gamarro, F.; Castanys, S.; Lopez, M. *J. Med. Chem.* **2008**, *51*, 7132−7143.

(3) Koulouri, S.; Malamidou-Xenikaki, E.; Spyroudis, S. *Tetrahedron* **2005**, *61*, 10894.

(4) (a) Manthey, M. K.; Pyne, S. G.; Truscott, R. J. W. *Aust. J. Chem.* **1989**, *42*, 365. (b) Ikeda, M.; Kitahara, K.; Nishi, H. *J. Heterocycl. Chem.* **1992**, *29*, 289. (c) Zhang, D.; Jin, G.-X. *Organometallics* **2003**, *22*, 2851. (d) Gellerman, G.; Rudi, A.; Kashman, Y. *Tetrahedron* **1994**, *50*, 12959. (e) Reuben, G.; Shonle, H. A. *J. Am. Chem. Soc.* **1946**, *68*, 2246. (f) Placin, F.; Clavier, G.; Najera, F.; Desvergne, J. P.; Pozzo, J. L. *Polycyclic Aromat. Compd.* **2000**, *19*, 107. (g) Lehaire, M.-L.; Scopelliti, R.; Herdeis, L.; Polborn, K.; Mayer, P.; Severin, K. *Inorg. Chem.* **2004**, *43*, 1609. (h) Seillan, C.; Brisset, H.; Siri, O. *Org. Lett.* **2008**, *10*, 4013. (i) Tang, Q.; Liu, J.; Chan, H. S.; Miao, Q. *Chem.—Eur. J.* **2009**, *15*, 3965. (j) Lee, D.-C.; Cao, B.; Jang, K.; Forster, P. M. *J. Mater. Chem.* **2010**, *20*, 867. (k) Tang, Q.; Liang, Z.; Liu, J.; Xu, J.; Miao, Q. *Chem. Commun. (Cambridge)* **2010**, *46*, 2977. (l) Di, C.; Li, J.; Yu, G.; Xiao, Y.; Guo, Y.; Liu, Y.; Qian, X.; Zhu, D. *Org. Lett.* **2008**, *10*, 3025.

(5) Indirect quantification of acetic acid by using the ratio between malonic acid and acetic acid is impossible in this case, since a substantial part of the protons of malonic acid is deuterized by D_2O during the degradation.

(6) We also optimized another transitions state connecting DHBQ to **I1k**, in which only two water molecules are involved. However, the calculated activation barrier (19.5 kcal/mol) was much higher than that of **TS1**, indicating that at least three water molecules are necessary to smoothly complete the nucleophilic addition; see also Figure S10 in Supporting Information.

(7) We did not calculated the transition states of this keto−enol interconversion, but the barriers in this process would be quite low, since the keto form is much more stable than the enol counterpart.

(8) One of the reasons for the discrepancy in the $\Delta^{\ddagger}S°$ is that we used the gas phase rotational entropy without correction, though we corrected the translational entropy.

(9) Siegel, B.; Lanphear. *J. Org. Chem.* **1979**, *44*, 942.

(10) (a) Dagaut, P.; Wallington, T. J.; Kurylo, M. J. *J. Phy. Chem.* **1988**, *92*, 3836. (b) Vaghjiani, G. L.; Ravishankara, A. R. *J. Phys. Chem.* **1989**, *93*, 1948. (c) Lightfoot, P. D.; Veyret, B.; Lesclaux, R. *J. Phy. Chem.* **1990**, *94*, 708. (d) Lightfoot, P. D.; Lesclaux, R.; Veyret, B. *J. Phy. Chem.* **1990**, *94*, 700. (e) Wallington, T. J.; Dagaut, P.; Kurylo, M. J. *Chem. Rev.* **1992**, *92*, 667.

(11) Frisch, M. J. et al. *Gaussian 09*, Revision A.1; Gaussian, Inc.: Wallingford, CT, 2009. See Supporting Information for the complete reference.

(12) (a) Becke, A. D. *Phys. Rev. A* **1988**, *38*, 3098. (b) Becke, A. D. *J. Chem. Phys.* **1983**, *98*, 5648.

(13) Mammen, M.; Shakhnovich, E. I.; Deutch, J. M.; Whitesides, G. M. *J. Org. Chem.* **1998**, *63*, 3821.